Vanadium additions in new ultra high strength and ductility steels.

SCOTT Colin, CUGY Philippe

(ArcelorMittal Research, Voie Romaine BP30320, 57283 Maizières-lès-Metz, France)

Abstract:. Kinetic thermodynamic modeling has been used to optimise the process parameters for microalloying high Mn austenitic TWIP cold strips with Vanadium and Nitrogen to promote an intense precipitation of sub 10 nm intragranular V(C,N) particles during the continuous annealing step. The yield strength increase is 500 MPa / % wt. added V. A further interest lies in the amelioration of hydrogen induced delayed fracture (DF) in regions of cold formed parts with critically high residual tensile stresses. The beneficial macroscopic effect on DF is clearly demonstrated; however the physical mechanism governing the interaction between Vanadium and mobile hydrogen is still the subject of investigation.
Key words: TWIP, high Mn, austenite, vanadium microalloying, residual stress, delayed fracture.

1. Introduction

Meeting the challenge of stricter CO_2 target emissions requires automotive manufacturers to achieve significant weight reductions in the vehicle body in white. Faced with this challenge, steel manufacturers are developing breakthrough products with lower densities and/or higher mechanical properties. One class of alloys of special interest at the moment is Fe-Mn-C austenitics which exhibit the TWinning Induced Plasticity (TWIP) effect. Like the Hadfield steels to which they are related, these grades exhibit remarkable strain hardening properties far in excess of other ferrous alloys and several steelmakers are actively developing these products[1-4]. In this paper we will discuss two areas where vanadium additions can be of great interest in TWIP steels. The first derives from the need to increase the yield strength of these materials without degrading the (already challenging) hot and cold rolling conditions. Vanadium microalloying is an ideal candidate to produce a fine, homogeneous dispersion of intragranular sub-10 nm particles which can be formed during the continuous annealing step after cold rolling and which can contribute up to +450 MPa to the yield strength. The second interest of vanadium precipitates lies in the positive effect on hydrogen induced delayed fracture. The combination of ultra high strength with extended formability found in TWIP grades inevitably leads to the production of cold formed parts with zones containing extremely high residual stress levels. If the concentration of mobile hydrogen in these zones exceeds a critical limit, the part can be susceptible to delayed cracking. Although the hydrogen content can be rigorously controlled at the production stage, mobile hydrogen may be introduced at later stages by welding, surface or heat treatments, corrosion etc. These factors cannot be controlled by the steelmaker. It is thus advantageous to introduce matrix trapping sites which can act as sinks for mobile hydrogen and hence reduce the risk of delayed cracking. Our research has shown that vanadium additions provide increased resistance to delayed cracking in high manganese austenitic steels.

2. Experimental Method

The heats described in this paper were cast as 15 kg ingots in a laboratory vacuum induction furnace and hot and cold rolled using the pilot facilities at ArcelorMittal Maizières, although material was industrially produced. As the objective is to produce cold strips, equilibrium thermodynamic calculations using the kinetic Multipreci model[5] were used to determine the optimum reheating conditions to ensure the complete dissolution of vanadium precipitates in the as-cast ingots and the hot rolling and coiling parameters were chosen in order to minimise the amount of vanadium precipitation in the hot strip:

- Reheating at 1180°C for 15 minutes in an argon atmosphere.
- Reduction from approximately 70 mm to a final thickness of 3 mm.
- End rolling temperature > 900°C.
- Fast water cooling (30°C/s) to the coiling temperature (< 400°C).

A pilot laboratory cold rolling mill was used to reduce the hot strip thickness from 3 mm to 1.5 mm (50% reduction). Continuous annealing simulations were applied to the full hard heats either in a high vacuum AET 1450 fast annealing simulator under a back filled Ar atmosphere (dew point < -60°C) or in a Bähr DIL805A plastodilatometer. Due to the fine grain size of these alloys the specimens were observed using either backscattered electron imaging (crystallographic contrast mode) or EBSD in the FEG-SEM. Final mirror polishing was done using the Struers OPS method. Quantitative determinations of grain sizes and recrystallised fractions were carried out using an Aphelion image analysis system. A Philips CM20 200kV FEG-TEM was used to characterise the precipitation state. All precipitates were analysed using carbon extraction replicas.

Quantitative image analysis of TEM micrographs for precipitate size distribution determination was carried out as follows: image magnification 66K, negatives scanned at 800 dpi, manual identification of precipitates using a graphical analysis package and finally quantitative image analysis of the manually treated images. Precipitate volume fractions were determined by selective chemical dissolution: samples were etched in hydrochloric acid and rinsed in methanol and then placed in an electrolytic bath containing lithium chloride and salicylic acid diluted in methanol. Approximately 1.5 g of metal was dissolved at an applied current density of 20 $mA.cm^{-2}$. The precipitates were recovered by passing the electrolyte through a polycarbonate filter of porosity 200 nm. The filter and precipitate residue were subsequently mineralised. Finally, the weight fraction of precipitated vanadium was quantified using a plasma torch coupled with an optical emission spectrometer (ICP-OES). The uncertainty is evaluated to be ±5 ppm wt. in the measurement range 10-100 ppm wt. and ±10 ppm wt. for values above 100 ppm wt. Mechanical testing was carried out using standard Vickers HV5 indentation analysis and ISO 12.5 x 50 tensile test specimens with a constant strain rate of $0.008s^{-1}$.

3. Results

Figure 1 shows true stress v true strain curves for a variety of Fe-Mn-C TWIP steels[6] in large grain (hot strip, D_γ > 10 µm) format. Two base compositions have been extensively investigated: Fe-22Mn-0.6C and Fe-17Mn-0.9C. The former is a (relatively) low carbon TWIP which is spot weldable with ferritic steels[2] and the latter shows the highest work hardening rate of any of the tested compositions[7].

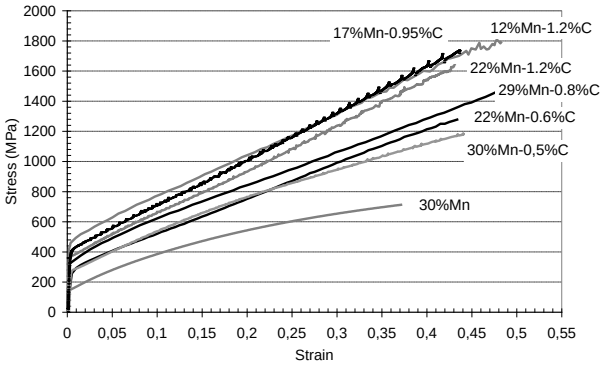

Fig.1 True stress v true strain curves for large grain Fe-Mn-C TWIP steels.

While the strain hardening coefficients of these compositions are remarkable, the yield stress is rather low, typically < ~400 MPa. Decreasing the grain size is an effective method for increasing the elastic limit – Figure 2 shows the variation in engineering stress v strain curves for Fe-22Mn-0.6C cold strips as the mean grain size is decreased. Unfortunately industrial process limitations in the cold rolling and annealing steps limit the minimum achievable grain size to 2.5 - 3 µm for this grade. Thus the maximum yield stress of cold strips is of the order of 450 MPa, whereas a reasonable target for high strength automotive applications is 600-700 MPa. It is therefore of interest to study the effect of precipitation strengthening in these steels.

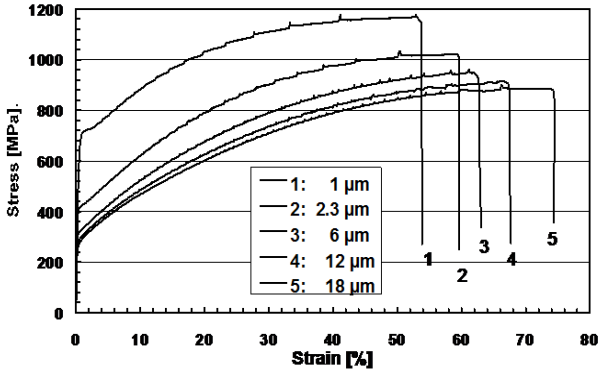

Fig.2 Engineering stress v strain curves for Fe-22Mn-0.6C as a function of grain size.

3.1 Precipitation hardening in Fe-Mn-C austenite

A limited amount of documentation exists in the literature concerning the precipitation of transition metal carbides in high manganese austenitic steels[8-25]. Most of the earlier data is related to attempts at precipitation strengthening in Hadfield steels. More recently there has been interest in hardening Fe-Mn based shape memory alloys. The first point of note is that, out of the eighteen studies listed, eleven concern V precipitation, five Nb precipitation, two (Ti+V) precipitation and only one Ti precipitation. Most of the articles describe experiments carried out on quenched ingots or hot rolled plates. Only three studies concern cold strips[8,19,22] however the precipitation heat treatments described are all incompatible with modern flat carbon production parameters. None of the authors determined the effect of high manganese concentrations on precipitate solubility products and, on the rare occasions where any precipitation calculations were made, standard literature values were taken. Few of the studies provide chemical extraction data for precipitate volume fractions and only one systematic TEM investigation of precipitate size histograms and number densities was found [22]. In conclusion, the literature results on precipitation in high manganese austenitic steels are open to limited qualitative interpretations only.

- The hardening effect of V is established [23,24]
- The hardening effect of Nb appears to be rather low at room temperature[8,12,14]
- There is insufficient data on Ti additions to draw any firm conclusions.

It is clear that the literature is of limited use in determining the optimum composition of carbide forming element and thermomechanical treatment for use in Fe-Mn-C TWIP cold strips. The first choice to make is which carbide forming element to use. Significant additions of Nb are likely to greatly increase the non-recrystallisation temperature T_{nr} during hot rolling. While this effect can be of benefit for ferritic steels (for grain refinement) any increase in hot rolling efforts for Fe-Mn-C TWIP steels could severely limit the attainable formats. Further, in preliminary laboratory experiments additions of 0.25% wt. Nb were found to provide only modest hardening in annealed cold strips (+50 MPa increase in YS and +30 MPa in UTS) in agreement with references[8,12,14]. This essentially leaves the choice between V and Ti. However, there are several practical reasons which mitigate in favour of the use of V.

The main concern centers around the different temperature domains of precipitation. Figure 3 shows the solubility products for various carbides and nitrides in austenite[26]. Note that these solubility products are not necessarily valid for high manganese steels. A few studies do exist concerning the effect of Mn on the established solubility products of VC[27,28]. Both authors found that increasing the Mn content increased the solubility of VC in austenite, but the effect appears to be rather small for Mn compositions up to 3% wt. No information is available at higher Mn contents.

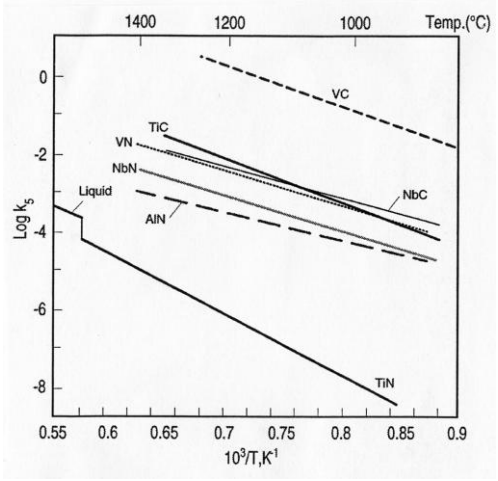

Fig.3 Equilibrium solubility products for microalloy carbides and nitrides in austenite[26].

Figure 3 shows that the solubility products of Ti and V are widely separated and thus it can be expected that the precipitation behaviour will be completely different in the two cases. Some Ti will precipitate out in the liquid phase as TiN if there is sufficient N present (we can expect around 100ppm of N in an industrial cast of Fe-Mn-C TWIP). Afterwards, Ti(C,N) and finally TiC will be formed as the slab is cooled. Those precipitates formed at high temperatures will be large (>50nm) and very stable – it will not be possible to redissolve TiN or large Ti(C,N) during the reheating stage. Whilst this is not a problem as regards hot rolling (large TiN precipitates do not introduce a precipitation strengthening effect and Ti in solution does not increase T_{nr} in the same way as Nb) most of the Ti which precipitates at high temperatures can be considered to be "lost" for our purposes. A further difficulty involves the formation of fine TiC precipitates during end rolling and coiling. The increase in the hot strip yield strength due to precipitation hardening (which can be up to +250 MPa in Ti microalloyed TRIP steels) may cause problems at the cold rolling stage[29].

Vanadium, on the other hand, is much simpler and more flexible to process. Any precipitates (VN, V(C,N) or VC) formed during casting will be redissolved during reheating. From previous work on Vanadium microalloyed TRIP steels[30], the solubility of V in austenite is such that there will be little or no V precipitation during hot rolling and coiling at temperatures below 500°C. Thus nearly all of the added V can be maintained in solid solution during the hot and cold rolling process (where any precipitation is problematic) remaining available to precipitate during continuous annealing. A great advantage of precipitation after cold rolling is that the precipitate distribution is intragranular and tends to be homogeneous – the most intense nucleation occurs on dislocations and shear bands during the initial heating stage before recrystallisation has been completed. In this way grain boundary precipitation (which would reduce ductility and toughness) is minimized.

3.2 Modelling the kinetics of V precipitation in austenite.

Successful optimization of the composition and thermomechanical treatment of microalloyed steels requires a detailed knowledge of precipitation kinetics. The Multipreci model developed at ArcelorMittal research has previously been successfully applied to describe V(C,N) precipitation in ferrite and austenite[30] and Nb(C,N) precipitation in ferrite[31]. Here the model input data for the solubility products of VC in austenite[32] and for VN in austenite [33] are respectively :

$$Log_{10} Ks\% = -9600/T + 6.72$$
$$Log_{10} Ks\% = -7840/T + 3.42$$

and the values for the diffusion coefficients of V, C, and N in austenite are[26]:

Vanadium : $D_0 = 0.25\ cm^2/s$, $Q = 264.2 kJ/mol$.
Carbon : $D_0 = 0.10\ cm^2/s$, $Q = 137.5 kJ/mol$.
Nitrogen : $D_0 = 0.91\ cm^2/s$, $Q = 168.6 kJ/mol$.

The interface energy is set constant equal to 0.5 J/m². Calculations were performed to compute the precipitation of V(C,N) of a Fe-Mn-C TWIP grade of composition: Fe-22Mn-0.2Si-0.6C-0.01N-0.2V. Figure 4 shows a calculated PTT diagram for V(C,N) precipitation during isothermal holding.

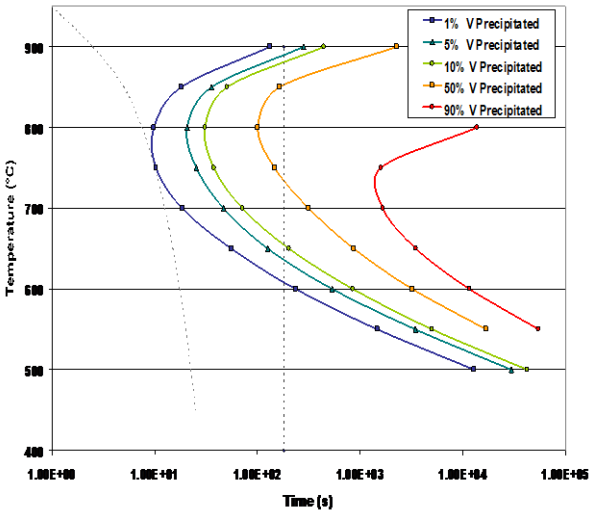

Fig. 4 Calculated PTT diagram for V(C,N) precipitation in Fe-22Mn-0.2Si-0.6C-0.01N-0.2V.

Several important points can be determined directly from an inspection of the PTT curves :

- The dissolution temperature of V(C,N) is ~900°C in this alloy so all V(C,N) precipitates formed during continuous casting will be redissolved during reheating.
- No V(C,N) precipitation can occur during hot rolling (assuming finish rolling at 950°C).
- After finish rolling a cooling rate of 20°C/s to coiling at a temperatures below 500°C (dotted curve) is sufficient to ensure that all the V remains in solid solution.
- Assuming a maximum continuous annealing hold time of 180 s (dotted line), the optimum temperature for V(C,N) precipitation at this composition is 800°C. Under these conditions approximately 70% (i.e. 0.14% wt.) of the available V is precipitated as V(C,N).

If we look at the precipitate distribution after continuous annealing at 800°C for 180 s we can see that the number density is constant in this region ($3x10^5$ precipitates / μm^3) signifying that nucleation has finished and that the precipitates are in the growth stage. The model predicts an average diameter of ~3nm for the V(C,N) precipitates, however this value is likely to be underestimated in reality as it does not take into account any precipitation during the heating cycle.

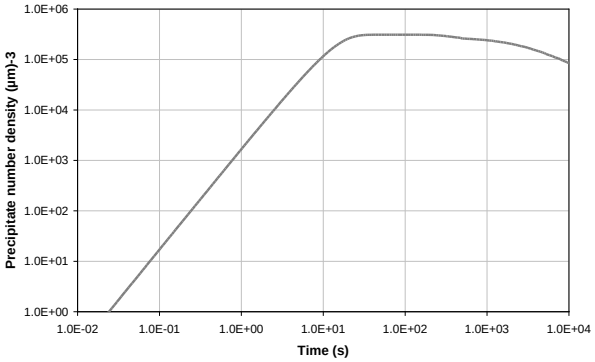

Fig. 5 Variation of the number density of V(C,N) precipitates with time in Fe-22Mn-0.2Si-0.6C-0.01N-0.2V held at 800°C.

Another important metallurgical factor is the reduction in matrix carbon concentration engendered by this precipitation. The model predicts that 0.023%wt. C is lost to precipitation at the end of an annealing cycle of 800°C / 180 s. Assuming an initial composition of 0.6%wt. C, the matrix composition will fall to 0.578% wt. This change is negligible from the point of view of the impact on the mechanical properties.

3.3 The influence of N concentration on V(C,N) precipitation kinetics.

The presence of N has a vital role in boosting the precipitation kinetics of V. In figure 6 we show the effect of increasing the N concentration from 10 ppm wt. (typical of a laboratory ingot) to 100 ppm wt. (typical of continuous cast slab) on the time required to precipitate 50% of the available vanadium. The result is quite clear – increasing the nitrogen concentration raises the temperature of the nose of the "C" curves (VN is less soluble in austenite than VC) and accelerates the kinetics of V precipitation. In this particular case the nose is shifted from <750°C to 800°C and the time necessary to precipitate 50% V decreases from 650s to 100s.

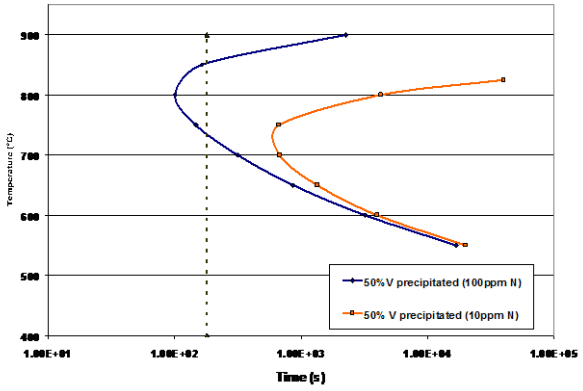

Figure 6. Calculated PTT diagram for 50% V(C,N) precipitation in Fe-22Mn-0.2Si-0.6C-0.2V containing 10 ppm wt. and 100 ppm wt. of N.

3.4 Microstructural investigations

The quantity of V precipitated in two industrial Fe-22Mn-0.6C-0.2V-0.01N hot coils where the finish rolling temperature was > 900°C and a fast cooling rate of 20°C/s was applied to achieve a coiling temperature < 300°C was measured. The values obtained varied between 28 ppm wt. and 61 ppm wt. for a calculated value of 51 ppm wt. confirming our calculations that, under these conditions, all of the V remains in solid solution in the hot strip. After 50% reduction by cold rolling and annealing for 180 s at 800°C the amount of V precipitated was 1164 ppm wt. +/- 87 ppm wt. i.e. 58% of the available vanadium. This figure represents the average of 57 measures made on 14 industrial coils. This is a little lower than the calculated value (1400 ppm wt.) suggesting that the solubility products for VC and VN are increased by the high Mn concentration.

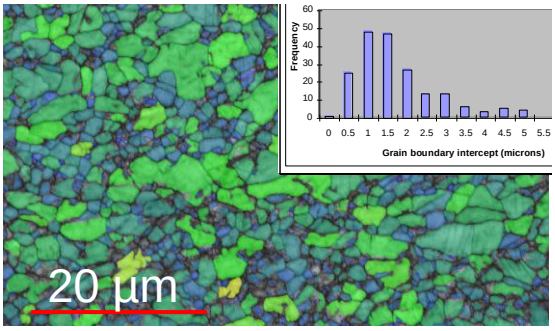

Fig. 7 Annealed cold strip microstructure for Fe-22Mn-0.2Si-0.6C-0.2V annealed at 800°C / 180 s. The mean grain size is < 2µm.

Figure 7 is an EBSD image of the annealed cold strip microstructure. The inset grain boundary intercept histogram confirms that the presence of vanadium has refined the grain size from ~3 µm to < 2 µm. Figure 8 is a TEM micrograph of an extraction replica showing the distribution of V(C,N) precipitates after annealing. The measured precipitate size histogram is also shown in the inset. The precipitates are small (mean radius = 3.6 nm), equiaxed and intragranular in nature. This figure has recently been confirmed by SANS data[34]. An inspection of Figure 8 reveals that some precipitates are aligned along prior dislocation lines (indicated by the arrow). This implies that precipitation starts early during the heating stage before recovery and recrystallisation are completed. This hypothesis is supported by Figures 9a and 9b where full hard cold strips were heated at 60°C/s and directly quenched at five temperatures between 570°C and 812°C. The recrystallised fraction and the amount of V precipitated were measured at each point. It is interesting to note that the slope of the recrystallisation curve is slowed at ~ 725°C. From Figure 9b this coincides exactly with a sharp increase in the vanadium precipitation kinetics.

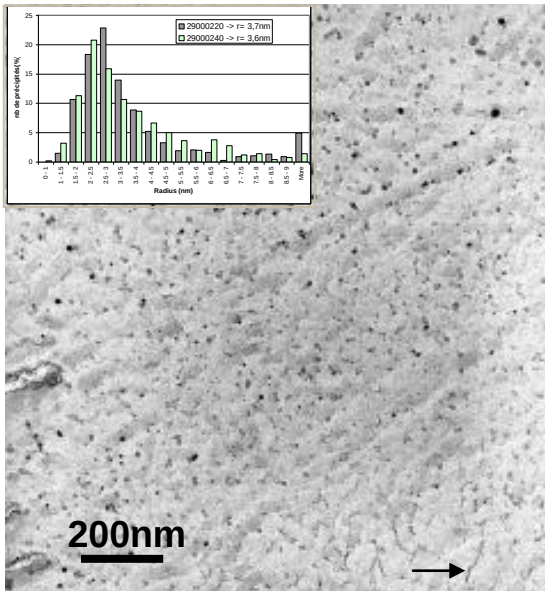

Fig. 8 TEM extraction replica showing V(C,N) from an industrial Fe-22Mn-0.2Si-0.6C-0.2V cold strip annealed at 800°C / 180 s.

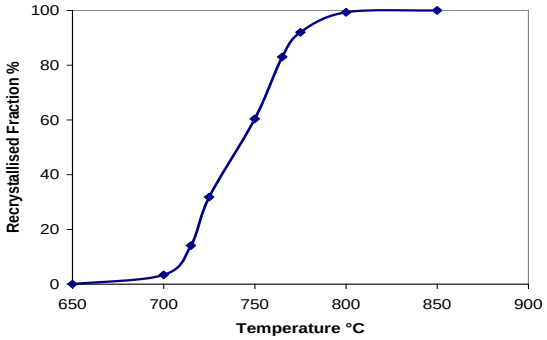

Fig. 9a Recrystallisation kinetics for industrial Fe-22Mn-0.2Si-0.6C-0.2V cold strip heated at 60°C/s

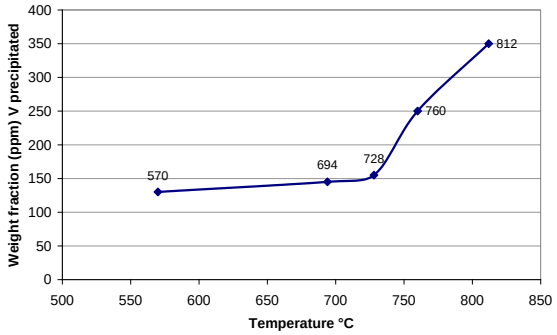

Fig. 9b Precipitated weight fraction (ppm) of V measured after quenching from the indicated temperatures.

Thus it is reasonable to assume that the processes of recrystallisation and precipitation must be concurrent.

3.5 Mechanical properties

The strengthening effect of vanadium microalloying in hot strips is limited. Figure 10 summarises the effect of V additions between 0 and 0.4% wt. on laboratory Fe-22Mn-0.6C hot bands. Essentially no effect is seen on the UTS, the total elongation is fairly constant and there is an increase in YS of ~200 MPa / %wt. V. This is probably due to a solid solution effect as the grain size is not much altered (from 8.5 µm without V to 7.5 µm with 0.4% wt. V).

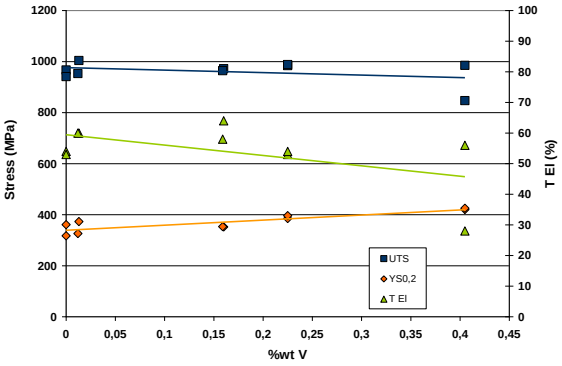

Fig. 10 Effect of V additions on the mechanical properties of Fe-22Mn-0.6C hot strips.

However there is a much larger difference in the cold strip behaviour when V is added. Figure 11 shows a direct comparison between the true stress/true strain curves for industrial coils with and without V microalloying (compositions Fe-22Mn-0.6C and Fe-22Mn-0.6C-0.2V-0.01N).

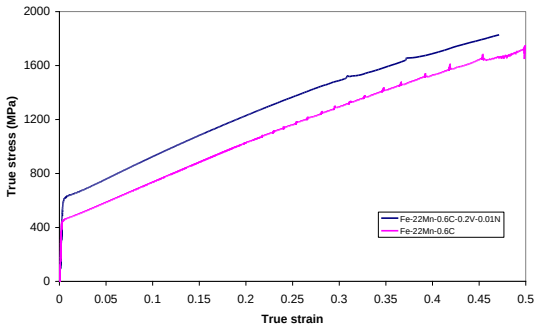

Fig. 11 Effect of V additions on the mechanical properties of Fe-22Mn-0.6C cold strips.

The increase in yield stress for an addition of 0.2% wt. V is +150 MPa and the increase in the UTS is +100 MPa. The fact that the two flow curves are essentially parallel shows that V microalloying does not modify the strain hardening mechanisms. This strong increase is due in no small part to the grain size refinement effect. In order to separate the contribution of precipitation strengthening and solid solution effects we have plotted the variation in yield strength as a function of cold strip grain size for the same two compositions (Figure 12). The data has been fitted with two Hall-Petch curves which are not parallel as the precipitated fraction and the size distribution of V(C,N) cannot be maintained constant when the cold strip grain size is varied by heat treatments and also hardening due to grain refinement and precipitation strengthening are not independent mechanisms especially at smaller grain sizes. At large grain sizes (> 5 µm) most of the V is in solid solution and the difference in yield stress is due to solid solution hardening. This is ~50 MPa for an addition of 0.2% wt. V or 250 MPa / % wt. V which is similar to the value found for the hot strips.

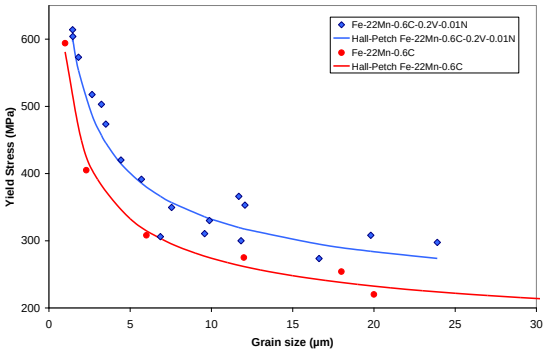

Fig. 12 Variation of yield stress with grain size for Fe-22Mn-0.6C cold strips.

At grain sizes below 3 µm the hardening due to V additions increases to almost 500 MPa / % wt. This remarkable figure has been confirmed by laboratory experiments on Fe-17Mn-0.9C alloys. Figures 13a and 13b show the increase in mechanical properties of annealed cold strips obtained by adding V up to 1% wt. An increase in yield stress of more than +450 MPa / %wt. V was obtained together with +350 MPa / %wt. V augmentation in UTS for a small reduction (<10%) in elongation.

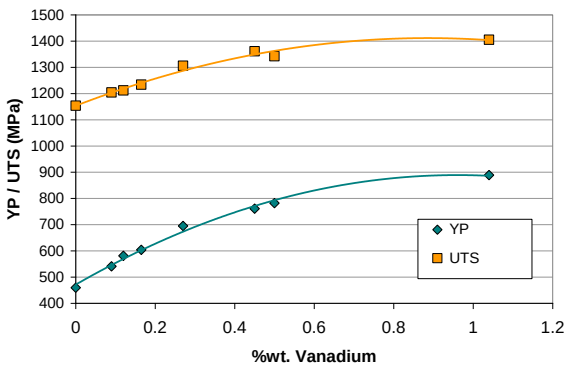

Fig. 13a Mechanical properties of Fe-17Mn-0.9C annealed cold strips with Vanadium additions

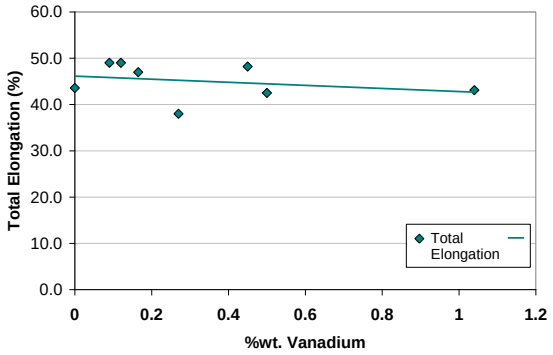

Fig. 13b Variation in ductility of Fe-17Mn-0.9C annealed cold strips with Vanadium additions

Thus with the appropriate V microalloying the yield stress can be varied between 470-900 MPa and the UTS between 1150-1400 MPa while maintaining a uniform elongation > 35%.

3.5 Effect on hydrogen embrittlement

Hydrogen induced delayed fracture is a potential problem for cold formed ultra high strength steels especially when the intrinsic hydrogen concentration is increased by hydrogen pickup during the electogalvanising process. Austenitic steels are particularly sensitive to this phenomenon as the hydrogen solubility is higher and the diffusion rate is much slower than in ferritics. Fe-Mn-C TWIP steels are no exception and Figure 14 shows a fully drawn cup (Fe-22Mn-0.6C drawing ratio β=1.8) where intergranular delayed fracture (DF) has occurred after forming.

Fig.14 Hydrogen induced delayed cracking in a Fe-22Mn-0.6C fully drawn cup.

Apart from the hydrogen content the principal factor governing the risk of DF in cold formed parts is the presence of residual tensile stresses. The results of a finite element calculation of residual stresses for the cup in Figure 14 can be seen in Figure 15.

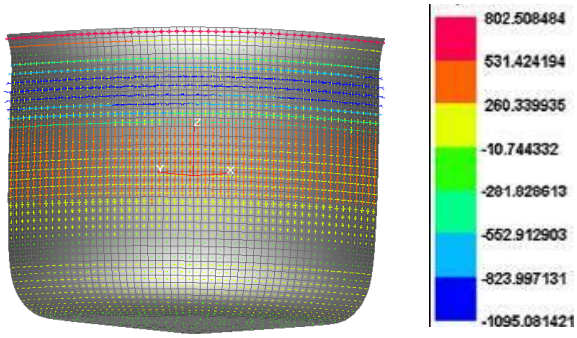

Figure 15: FEM simulation of residual stresses in a Fe-Mn-C TWIP fully drawn cup. The colour scheme represents the intensity of the major stress component on the outer fiber. Blue is compressive and red represents tensile stresses.

Evidently the residual stress distribution is complex and varies from compression to tension at different heights in the cup wall. Figure 16 shows the variation in hoop stress along a curvilinear axis taken parallel to the rolling direction starting at the centre of the cup base (0 mm) and ending at the cup rim (76 mm). Four curves are plotted, one each for the inner wall, the outer wall, the neutral fiber and one (red diamonds) representing the average of the other three. This latter curve has recently been validated by high energy synchrotron transmission X-ray diffraction[35]. It is important to note that, after springback, the residual hoop stress configuration at the cup rim is tensile at all points in the sheet thickness with a magnitude > 1000 MPa.

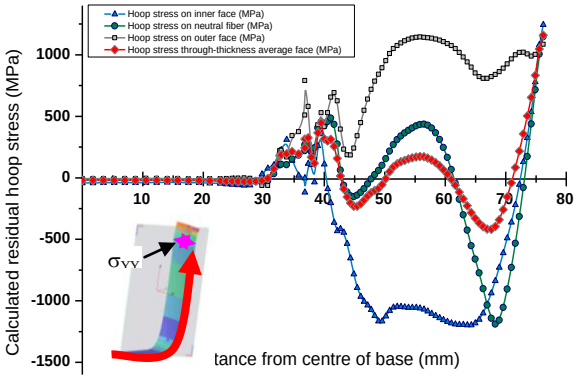

Fig.16 : Calculation of residual hoop stresses in a fully drawn cup on the outer fiber (squares), on the neutral fiber (circles) and on the inner fiber (triangles) along a curvilinear abscissa parallel to RD. The diamonds represent the average through-thickness stress.

In the presence of a critical concentration of mobile hydrogen, estimated to be ~2ppm wt. for Fe-22Mn-0.6C, the residual stress conditions at the cup rim are severe enough to provoke delayed cracking. A simple test can thus be devised where the time to cracking of fully drawn cups

compressed in a vice (to speed up the test) is monitored.

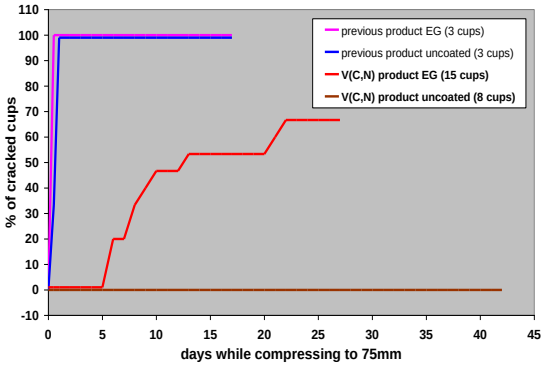

Fig.17 Evolution of delayed cracking in fully drawn cups (uncoated and electrogalvanised) for Fe-22Mn-0.6C and Fe-22Mn-0.6C-0.2V-0.01N.

In Figure 17 the evolution of DF for two alloys, Fe-22Mn-0.6C and Fe-22Mn-0.6C-0.2V-0.01N using this test is shown. For the non-microalloyed steel all of the cups (coated and uncoated) cracked in less than 1 day. For cups made from the V microalloyed composition cracking was completely suppressed in uncoated cups and strongly reduced in electrogalvanised cups (note that the ambient humidity was < 60% during these experiments). This is all the more encouraging as V additions increase the mechanical properties and thus the residual stress in the formed part. Another positive factor is that not only the risk but also the intensity of DF was reduced.

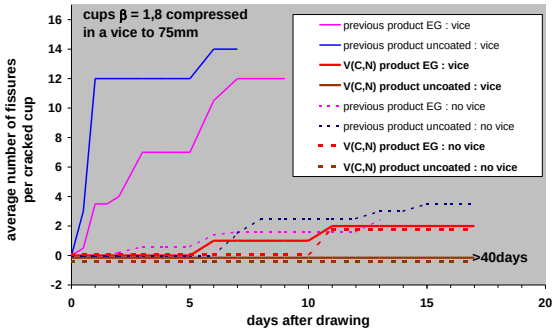

Fig.18 : Evolution of the intensity of delayed cracking in fully drawn cups (uncoated and electrogalvanised) for Fe-22Mn-0.6C and Fe-22Mn-0.6C-0.2V-0.01N.

In Figure 18 we plot the average number of cracks per cup as a function of time. The standard TWIP steel shows up to 12 cracks per cup in electrogalvanised material whereas with electrogalvanised V microalloyed sheets only 1 or 2 cracks per cup were found.

4. Conclusions and future work

The results presented here show conclusively that there is a strong interest in microalloying high Mn TWIP steels with vanadium. The yield strength increase in continuously annealed cold strips is 500 MPa / % wt. of V addition. This figure can be decomposed into ~250 MPa solid solution hardening and ~250 MPa due to grain refinement and precipitation strengthening. Thermodynamic kinetic modelling has been used to optimise the thermomechanical parameters and obtain an intense precipitation of sub 10 nm strain-induced intragranular V(C,N) particles which form during continuous annealing step after cold rolling. This has the advantage that casting and hot rolling properties are virtually unaffected and the final mechanical properties in the finished coil are constant due to the homogeneous precipitate distribution. By careful control of the N concentration it is possible to precipitate 58% of the added V even though the annealing cycle is short (180 s). In a practical case we have shown that, for the alloy Fe-17Mn-0.9C which shows the highest strain hardening coefficient of any of the TWIP alloys tested, the yield stress can be varied between 470-900 MPa and the UTS between 1150-1400 MPa by V additions of up to 1% wt. while maintaining a consistent uniform elongation > 35%.

A further interest in V precipitates lies in the amelioration of hydrogen induced delayed fracture in regions of cold formed parts where critically high residual tensile stresses are present. While the macroscopic effect on DF has clearly been demonstrated, the physical mechanism governing the interaction between V precipitates and mobile hydrogen in steels is not clear. We have carried out extensive studies using the 3D Tomographic Atom Probe (TAP) to obtain images of precipitates in samples containing hydrogen and deuterium. Although it was possible to detect both precipitates and individual hydrogen and deuterium atoms, no convincing evidence of any conventional trapping mechanism was found by this method. Our current work is now centered around Small Angle Neutron Scattering (SANS) and Thermal Desorption Analysis (TDA). A deeper understanding of this mechanism is necessary as, while V additions are certainly useful, they are not yet sufficient on their own to guarantee critical part integrity, especially in conditions where external sources of hydrogen (e.g. electrogalvanised coatings or surface corrosion) are present. The successful commercial implementation of TWIP steels will depend on this point.

5. Acknowledgements

The authors would like to thank numerous collegues at ArcelorMittal Research for their help and support; O.Bouaziz for the TWIP data in Figure 1, D.Barbier for the EBSD measurements, S.Beurrot for the recrystallisation data, P.Dietsch for the FEM calculations, P.Barges for the TEM analysis and G.Petitgand and B.Remy for the thermomechanical treatments.

References:

[1] Fommeyer G, Drewes E J, Engl B. Physical and Mechanical properties of iron-aluminium (Mn, Si) lightweight steels. La Revue de Metalliurgie-CIT Oct 2000: 1245–1253.

[2] Scott C, Allain S, Faral M, Guelton N. The development of a new Fe–Mn–C austenitic steel for automotive applications. La Revue de Metalliurgie-CIT 2006 103 : 293–302.

[3] H Hofmann, M Menne, S Göklü, H Richter. Proc. of International Conference on Steel Future for the Automotive Industry, Wiesbaden, Germany, 2005 : 73-80.

[4] Chen L. et al. Localized Deformation due to Portevin–LeChatelier Effect in 18Mn–0.6C TWIP Austenitic Steel. ISIJ International, 2009, 47 (12) : 1804–1812.

[5] Maugis P, Gouné M, A computer model of carbonitride precipitation in steel, Proc. of IAC3 conference, Estoril, Jul. 2002.

[6] Bouaziz O, et al. 2009 submitted to Scripta Mat.

[7] Cugy P, et al, Method of producing austenitic iron/carbon/manganese steel sheets having very high strength and elongation characteristics and excellent homogeneity. Patent WO 2006/056670.

[8] Chaturvedi M C, Honeycombe R W K, Warrington D H, Stacking Fault Precipitation of NbC in Iron-Manganese Austenites, J. Iron and Steel Inst. Dec.1968 : 1236-1244.

[9] Matveev Yu G, Bukhtin V S, Tarasko D I, Hardening during explosive shock loading of steel 110G13L alloyed with Vanadium and modified with Titanium. Metallovedenie I Termicheskaya Obrabotka Metallov, 1975, 3 : 51-53.

[10] Harris S J, Nag N R, Effect of warm working on the precipitation of vanadium carbide in a medium carbon austenitic steel, J.Mat.Sci., 1976, 11 : 1320-1329.

[11] Miska K H, Consider Austenitic Manganese Steels for Impact and Wear Applications, Mat.Eng. 1977, 8-77 : 42-44.

[12] Masumoto H, et al. Development of High-Manganese Steels. Nippon Steel Technical Report 1983, 22 : 47-59.

[13] Atasoy O A et al. Effect of alloying elements and heat treatment on the structure and properties of Hadfield's austenitic manganese steel. Z.Metallkde. 1984, 75 : 463.

[14] Kim Y G, Park Y S, Han J K, Low temperature mechanical behaviour of microalloyed and controlled rolled Fe-Mn-Al-C-X Alloys. Met.Trans A. 1985, 16A : 1689-1693.

[15] Atasoy O A, et al. Precipitation of vanadium carbides in 0.8%C-13%Mn-1%V austenitic steel. J.Mat.Sci., 1989, 24, : 1393-1398.

[16] Hee Han K, The microstructures and mechanical properties of an austenitic Nb-bearing Fe-Mn-Al-C alloy processed by controlled rolling. Mat.Sci.Eng. 2000, A279 : 1-9.

[17] Guo Z, et al. The influence of (MnS+VC) complex precipitates on the crystallography of intergranular pearlite transformation in Fe-Mn-C hypereutectoid alloys. Scripta Mat., 2001, 45 : 525.

[18] Kajiwara S. et al. Remarkable improvement of shape memory effect in Fe-Mn-Si based shape memory alloys by producing NbC precipitates. Scripta Mat.,2001, 44, : 2809-2814.

[19] Guo Z, et al. Kinetics and crystallography of intragranular pearlite transformation nucleated at (MnS+VC) complex precipitates in hypereutectoid Fe-Mn-C alloys. ISIJ Int. 2002, 42 (9) : 1033-1041.

[20] Furuhara T, et al. Multiphase crystallography in the nucleation of intragranular ferrite on MnS+V(C,N) complex precipitates in austenite. ISIJ 2003, 43 (12) : 2028-2037.

[21] Kubo H, et al. Characterisation of Fe-Mn-Si-Cr shape memory alloys containing VN precipitates. Mat.Sci.Eng. 2004, 378 (1-2) : 343-348.

[22] Yazawa Y, et al. Effect of matrix recrystallisation on morphology, crystallography and coarsening behaviour of vanadium carbide in austenite, Acta Mat. 2004, 52 : 3727-3736.

[23] El-Faramawy H, Effect of titanium and vanadium additions on high manganese (Hadfield) steel containing nitrogen, Steel Grips 2005, 3 (5) : 360-369.

[24] Sagaradze V V, et al. High Strength precipitation-hardening austenitic Fe-Mn-V-Mo-C steels with shape memory effect. Mat.Sci.Eng. 2008, A481-482, : 747-751.

[25] Srivastava A K, Das K, Microstructural and mechanical characterization of in situ TiC and (Ti,W)C-reinforced high manganese austenitic steel matrix composites. Mat.Sci.Eng. A 2009, 516 : 1-6.

[26] Gladman T, The Physical Metallurgy of Microalloyed Steels, The Institute of Materials. 1997.

[27] Huang W. Thermodynamic properties of the Fe-Mn-V-C system. Met.Trans. A, 1991, 22A : 1911-1920.

[28] Han K, Alloy additions on the solubility of alloy carbides in steels. Scripta Met. 1992, 28 : 699-702.

[29] Drillet J, Gouné M, TRIP 1000 microallié au titane en TAF : mécanismes métallurgiques. ArcelorMittal internal report 2002, CMC/02/R/3135

[30] Perrard F, Scott C, Vanadium Precipitation During Intercritical Annealing in Cold Rolled TRIP Steels. ISIJ Int. 2007, 47 (8) : 1168-1177.

[31] Maugis P, Goune M, et al. A model for niobium carbonitride precipitation in ferrite. Proc. of THERMEC 2003, Madrid, 2 : 1313-1318.

[32] Taylor K A, Solubiity products for titanium-,vanadium-,and niobium-carbide in ferrite. Scripta Met. et Mat. 1995, 32 : 7-12.

[33] Turkdogan E T, Causes and effect of carbide and carbonitride precipitation during continuous casting. Trans. ISS, Iron and steel maker, 1989 : 61-75.

[34] Malard B, ArcelorMittal internal report, 2009.

[35] Scott C, et al. Measuring Residual Stresses In Cold Formed Sheets by Synchrotron X-ray Diffraction. ArcelorMittal internal report, 2009.